

A New Type Of Fast-Switching Dual-Mode Ferrite Phase Shifter

William E. Hord, Charles R. Boyd, Jr., and Daniel Diaz
Microwave Applications Group, Santa Maria, California

Abstract — A new type of dual-mode phase shifter which uses a transversely magnetized variable field section is described. The device retains the features of the conventional dual-mode phase shifter—low insertion loss, moderate amplitude modulation, adequate frequency bandwidth, simple physical geometry—which allow it to be considered for use in two-dimensional scanning arrays. However, because of the transverse magnetizing field, the shorted-turn resistance is increased which results in either reduced switching time or reduced switching energy when compared with the conventional dual-mode unit which utilizes a longitudinal magnetizing field.

I. INTRODUCTION

The dual-mode phase shifter is shown conceptually in Fig. 1. The conventional dual-mode phase shifter uses the interaction of circularly polarized waves with longitudinally magnetized ferrite. For this design, the circulators of Fig. 1 are realized by permanent-magnet quadrupole field quarter-wave plate sections on either end of the variable field section. These quarter-wave plate sections convert linear polarization nonreciprocally to circular polarization nonreciprocally to circular polarization and vice versa. A more detailed description is available in the literature [1], [2]. The new design of interest here uses a transversely magnetized ferrite-filled waveguide to realize the nonreciprocal phase shifters of Fig. 1. There are two major differences between the new design and the conventional dual-mode design:

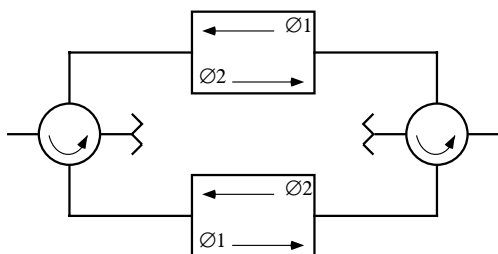


Fig. 1 Basic concept of the dual-mode ferrite phase shifter

- 1) The RF field propagating through the phase shift section is linearly polarized rather than circularly polarized.
- 2) The transverse magnetic bias field reduces the switching shorted-turn damping time constant.

Figure 2 shows block diagram of the longitudinal-field dual-mode phase shifter and two new realizations using the transverse field section. Figure 2(b) allows operation with linearly polarized energy, while Fig. 2(c) is designed for circularly polarized waves. The “nonreciprocal polarizers” consist of 45° Faraday rotators at either end of the phase shift section in Fig. 2(b), while quadrupole field magnetic quarter-wave plates are used for the realization of Fig. 2(c).

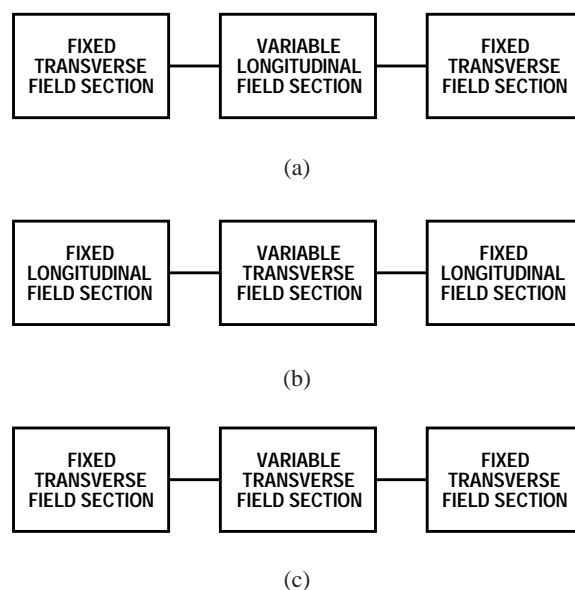


Fig. 2 Block diagram of dual-mode ferrite phase shifters. (a) Conventional dual-mode phase shifter. (b) The dual circuit of the conventional dual-mode phase shifter. (c) Another realization of the dual circuit.

The geometry of the transverse-field phase shifter is given in Fig. 3. A four-piece latching yoke is arranged to provide a quadrupole bias field in the microwave ferrite. A y-polarized TE₁₁ mode will exhibit different propagation constants for waves traveling in the +z direction and the -z direction. However, the symmetry is such that an x-polarized TE₁₁ mode traveling in the -z direction will have the same propagation constant as a y-polarized TE₁₁ mode traveling in the +z direction. The analysis given below closely parallel that of an earlier paper [3] which has not been widely distributed.

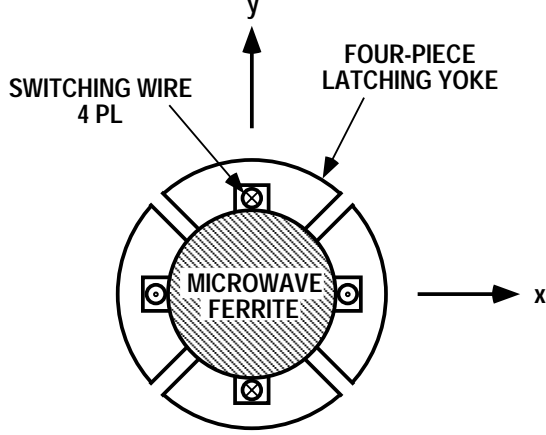


Fig. 3 Geometry of transverse field section

II. RF DESIGN CONSIDERATIONS

For a fully filled guide with transverse magnetization, the nonreciprocal differential phase shift $\Delta\phi$ is given by a relationship of the form

$$\Delta\phi = A\phi_0 \frac{f_c}{f} \frac{\kappa}{\mu} \quad (1)$$

where κ and μ are effective values of the permeability tensor for the magnetized ferrite, f_c is the cutoff frequency of the waveguide, f is the operating frequency, ϕ_0 is the insertion phase for a TEM wave propagating through the same length in the same medium, and A is a proportionality factor accounting for the relative effectiveness of the waveguide and bias field distributions. For example, A can be computed as equal to $4/\pi$ for a simple rectangular waveguide with equal and opposite uniform bias field level over the right and left halves of the guide. The mathematics leading to (1) have been derived on a basis of a transmission line equivalent-circuit model [4].

The insertion phase ϕ_0 can be expressed as

$$\phi_0 = \beta_0 l_p = \frac{360f \sqrt{\mu_r \epsilon_r}}{c} l_p \quad (2)$$

with l_p defined as the length of the phase shift section; furthermore

$$f_c = \frac{c}{\lambda_c \sqrt{\mu_r \epsilon_r}} \quad (3)$$

and for a circular waveguide $\lambda_c = 1.705 D$, giving

$$\Delta\phi \cong 211A \frac{l_p}{D} \frac{\kappa}{\mu} \text{ degrees} \quad (4)$$

where D is the guide diameter.

When the rod is magnetized by a weak applied field, κ and μ can be approximated by (5)

$$\kappa \cong \frac{M}{M_s} \frac{\omega_m}{\omega} \quad (5)$$

$$\mu = \mu_i + (1 - \mu_i) \frac{\tanh\left(1.25 \frac{M}{M_s}\right)}{\tanh 1.25} \quad (6)$$

where μ_i is the initial permeability, given by

$$\mu_i = \frac{1}{3} + \frac{2}{3} \sqrt{1 - \frac{(\omega_m)^2}{\omega^2}} \quad (7)$$

If the applied field is large enough to saturate the rod completely, then κ and μ are most appropriately taken as

$$\kappa \approx \frac{-M}{M_s} \left(\frac{\omega \omega_m}{\omega_0^2 - \omega^2} \right) \quad (8)$$

$$\mu = 1 + \frac{\omega_0 \omega_m}{\omega_0^2 - \omega^2} \quad (9)$$

In the above equations, ω is the operating radian frequency, ω_m is the material characteristic radian frequency, equal to the product of the gyromagnetic ratio and the saturation moment, and ω_0 is the resonance frequency given by Kittel's equation:

$$\omega_0 = \sqrt{\left\{ \mathcal{H}_0 + (N_x N_z) \omega_m \right\} \left\{ \mathcal{H}_0 + (N_y - N_z) \omega_m \right\}} \quad (10)$$

Here γ is the gyromagnetic ratio, H_0 is the externally applied field (z -directed), and N_x , N_y and N_z are demagnetizing factors for the ferrite shape.

The phase shift sections of concern here are ideally designed to operate up to the “knee” of the magnetization curve to achieve maximum available phase shift. This peak operating point does not apparently conform to either the “weak bias” or “strong bias” case described above. However, experimental studies have yielded the following observations:

- 1) The coefficient A is numerically equal to about 1.23.
- 2) The “weak bias” model fits experimental data reasonably well for $M/M_s \leq 0.25$. Above this level, a smooth transition begins toward the “strong bias” model.
- 3) The “strong bias” model gives a good fit to experimental data for M/M_s values near the “knee” of the magnetization curve.

Proceeding on this basis, take $\gamma H_0 = \omega_m M/M_s$ in (10) and note that for a long rod transversely magnetized, with the x direction along the rod axis

$$N_x = 0 \quad N_y = N_z = \frac{1}{2}. \quad (11)$$

Then substitute into (10) to get

$$r \equiv \frac{\omega_0}{\omega_m} = \sqrt{\frac{M}{M_s} \left(\frac{M}{M_s} - \frac{1}{2} \right)}. \quad (12)$$

Now it is possible to form the ratio κ/μ by substituting back into (8) and (9) after some manipulation obtain

$$\frac{\kappa}{\mu} \equiv \frac{M}{M_s} \frac{m}{1 - m^2 r(1 + r)} \quad (13)$$

where $m \equiv \omega_m/\omega$ and r is defined by (12) above. Then using $A = 1.23$, (4) for $\Delta\phi$ becomes

$$\Delta\phi = 260 \frac{l_p}{D} \frac{M}{M_s} \frac{m}{1 - m^2 r(1 + r)}. \quad (14)$$

Normalized curves relating maximum differential phase shift to m and M/M_s ratios have been plotted in Fig. 4 using this relationship.

The general form of (4) and (14) shows that for fixed values of all other parameters, the length of the phase shift section will be proportional to the ferrite rod diameter. Figure 5 indicates this relationship for a C-band design using various levels of ferrite material saturation moment, where a maximum phase shift of 500° and a peak M/M_s value of 0.75 have been assumed for configurations incorporating 45° Faraday rotators at each end.

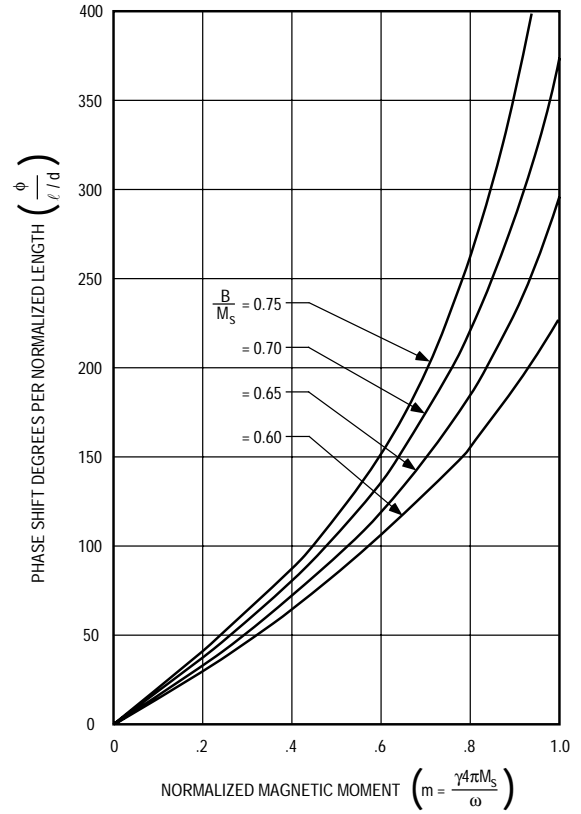


Fig. 4 Performance of differential phase shift section

As a consequence of the dependence of length on diameter, an optimum diameter value exists which minimizes the insertion loss for a given ferrite material. For smaller diameters, the conductive, dielectric, and magnetic losses rise at a faster rate than the length reduction, and so the net loss increases; the opposite situation occurs as the diameter is increased above the optimum value, although the rate of increase tends to be more gradual. The existence of an optimum diameter value is in contrast with the longitudinal field dual-mode phase shifter, for which insertion loss decreases monotonically with diameter up to the point of onset of high order modes that cannot be suppressed. Figure 6 shows plots relating insertion loss to diameter for the previous C-band design. These computations were made using the same perturbational relationships and material property assumptions as in previous studies for longitudinal field configurations. In common with the longitudinal field type, an optimum value for ferrite material saturation moment exists which minimizes insertion loss, although the value for the transverse field case is lower. Figure 7 demonstrates the existence of this optimum value, giving curves of insertion loss versus saturation moment at selected rod diameters at C-band. In summary, Figs. 8 and 9 show optimum diameter and optimum saturation moment values as functions of frequency.

The transverse field interaction for a fully filled waveguide is generally more frequency dependent than the longitudinal field interaction; hence frequency dispersion

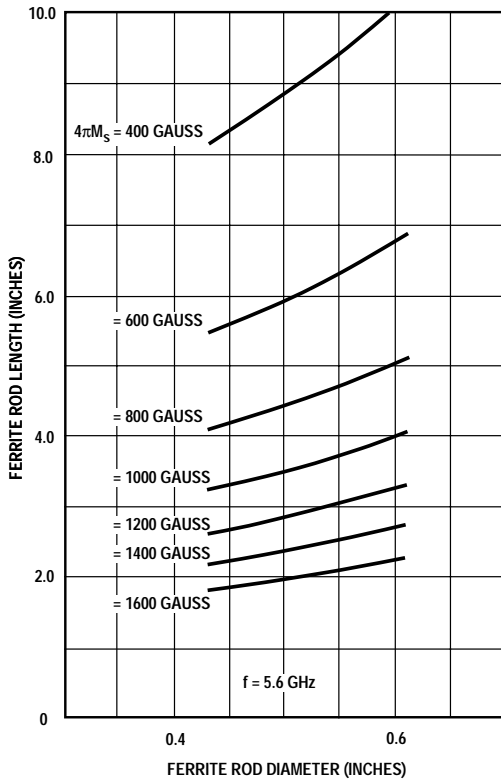


Fig. 5 C-band transverse-field dual-mode phase shifter ferrite rod design data

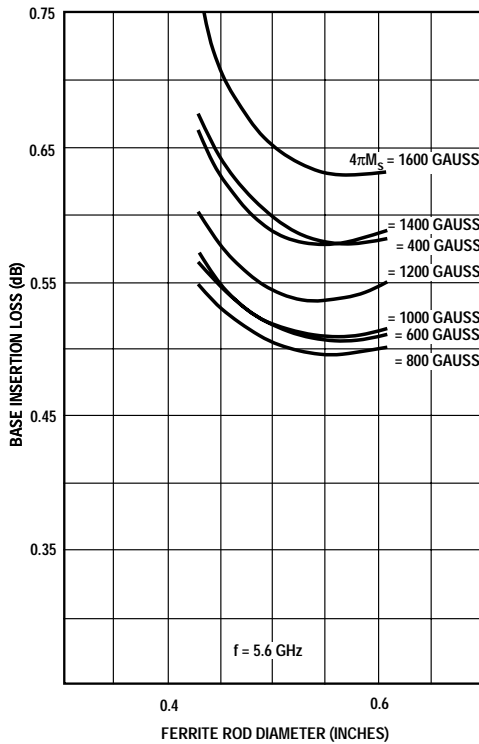


Fig. 6 C-band transverse-field dual-mode phase shifter loss dependence on rod diameter for various ferrite saturation moments

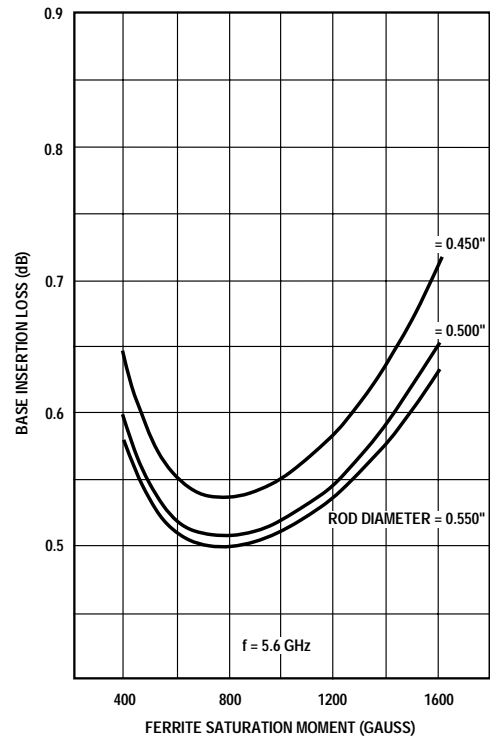


Fig.7 C-band transverse-field dual-mode phase shifter loss dependence on saturation moment for selected rod diameters

of phase shift values will be greater. Figure 10 shows a family of curves relating deviation of available band-edge phase shift from nominal as a function of fractional bandwidth for selected band-center ω_m/ω values. As with the longitudinal field case [6], modulation of insertion loss will occur with deviation of the polarizers or Faraday rotators, although the smaller frequency dependence of the latter will yield less band-edge modulation over the same frequency range. Hence, for the configuration using Faraday rotators, it appears that a smaller insertion loss modulation is exchanged for a greater dispersion of phase shift characteristics.

III. SWITCHING CONSIDERATIONS

One of the important features of the dual-mode phase shifter is the fact that the switching wires and the latching yoke are removed from the microwave circuit. This results in fairly simple fabrication and assembly of the phase shifter. However, the switching performance of the device is affected by eddy currents induced in the waveguide walls whenever the magnetic flux of the bias field is changed to produce phase shift. Prior study [6] of the longitudinal field dual-mode phase shifter has shown energy increases dramatically when the switching time is reduced below a particular reference time, defined as the “shorted-turn” damping time constant, which is determined by the structure dimensions and by the resistivity and thickness of the waveguide walls. The transverse field dual-mode device exhibits similar behavior, but the reference time is signifi-

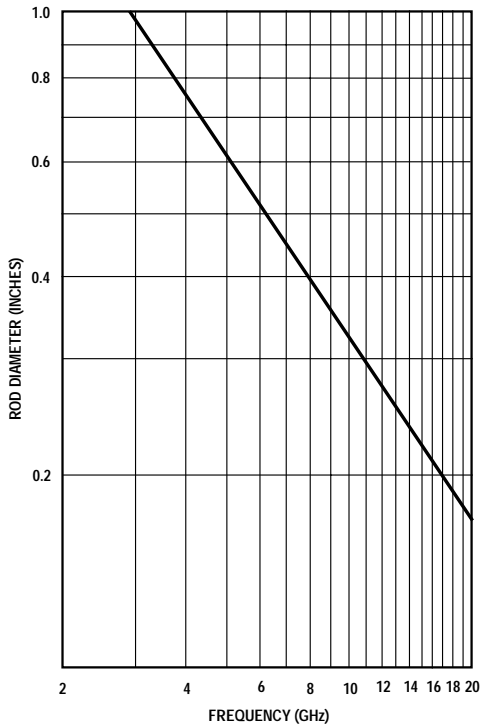


Fig. 8 Transverse-field dual-mode phase shifter optimum-loss rod diameter versus frequency

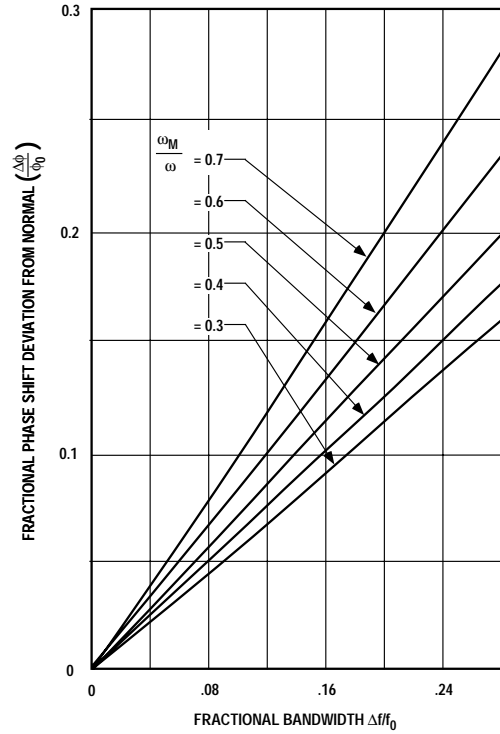


Fig. 10 Frequency dispersive deviation of available phase shift for transverse-field dual-mode ferrite phase shifter

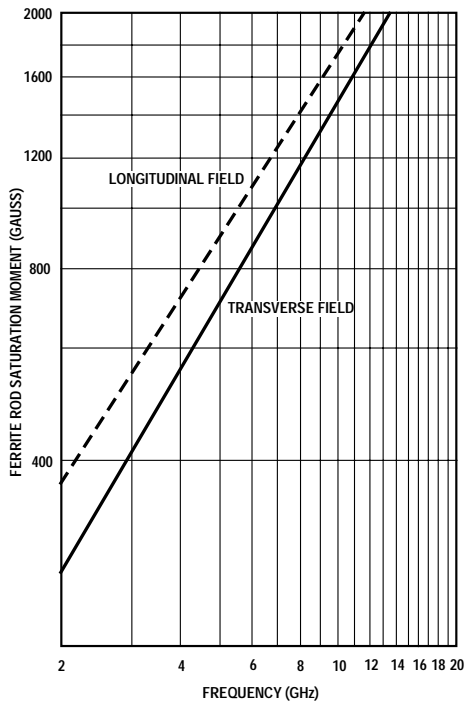


Fig. 9 Ferrite saturation moment versus frequency for loss-optimized dual-mode phase shifters

cantly reduced compared with the longitudinal field device.

The switching cycle consists of a “reset” portion followed by a “phase set” portion, as indicated in Fig. 11. It is assumed that partial switching of the core is accomplished by controlling the volt-time integral of the driver output pulse. The following analysis determines switching energy as a function of switching time as the flux is changed from the maximum negative value to the maximum positive value.

Consider a ferrite rod which has been metallized to form a waveguide. Onto this is placed a winding of N turns and a latching yoke. This assembly may be modeled by the circuit shown in Fig. 12. Here R_C is the effective resistance of the ferrite core during switching, L is the inductance of the assembly, and R_{st} is the shorted-turn resistance of the waveguide metallization multiplied by N^2 to reflect its apparent value in the primary circuit of the $N:1$ transformer. To change the flux from its maximum negative remanent value to its maximum positive remanent value, a constant voltage V is applied for a time T . The energy to switch the ferrite is

$$W_H = 2B_{max}H_C\Lambda \quad (15)$$

where B_{max} is the maximum remanent flux density, H_C is the coercive force, and Λ is the volume of ferrite being switched. This may also be written $W_H = V^2T/R_C$. The

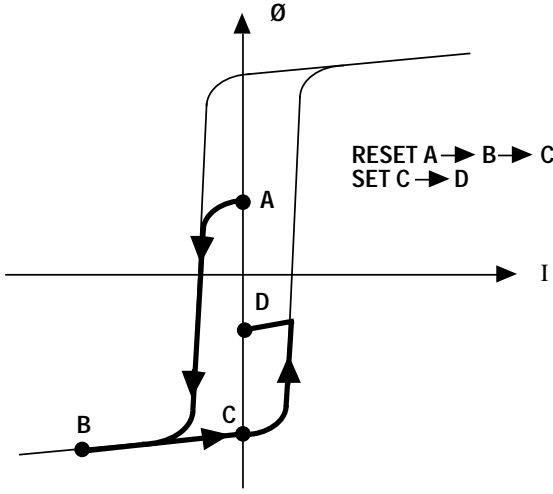


Fig. 11 Ferrite hysteresis loop showing switching cycle

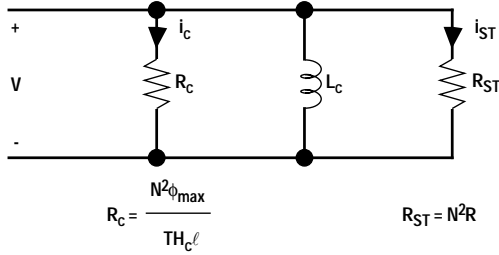


Fig. 12 Ferrite equivalent circuit during switching

energy dissipated by the eddy currents may be written $W = V^2 T / R_{ST}$ so that the total energy furnished is

$$W = W_H \left(1 + \frac{R_c}{R_{st}} \right) = W_H \left(1 + \frac{\tau}{T} \right) \quad (16)$$

where τ is the reference time, e.g. the shorted-turn damping time constant. The core resistance R_c is proportional to the square of the turns ratio, which means that the ratio of R_c to R_{st} is independent of the turns ratio. The effective resistance of the ferrite core may be adjusted through the turns ratio to present a wide range of levels to the electronic driver without changing the energy requirement, as long as the switching time T is held constant.

The length and diameter of the switched ferrite are approximately the same for the transverse field device and the longitudinal field device. Let D represent the diameter of the microwave ferrite, l the length and S the thickness of the metallization, and ρ the resistivity of the metallization. The following are easily derived for the longitudinal field device:

$$R_c = \frac{\pi D^2 N^2 B_{\max}}{4TH_c l} \quad R_{st} = \frac{\pi D^2 N^2 \rho}{sl} \quad \tau = \frac{SDB_{\max}}{4\rho H_c} \quad (17)$$

The distribution of the magnetic flux for the transverse-field device is shown in Fig. 13(a). During switching the spatial distribution of the time rate of change of the magnetic flux density is shown in Fig. 13(b). This results in an induced electric field density as shown in Fig. 13(c) and eddy currents as shown in Fig. 13(d). The current density is obtained from the electric field intensity through multiplying by the conductivity of the waveguide walls. The total eddy currents are found by integrating the current density.

Let N be the number of turns in a single slot of the yoke. Utilizing the fourfold symmetry of the geometry, the resistances and time constant may be calculated to be

$$R_c = \frac{\pi N^2 l B_{\max}}{4TH_c} \quad R_{st} = \frac{32N^2 \rho l}{\pi S D} \quad \tau = \frac{\pi^2 SDB_{\max}}{128\rho H_c} \quad (18)$$

The fringing fields at either end of the yoke have been ignored in the calculation of the shorted-turn resistance. However, these will increase the shorted-turn resistance so

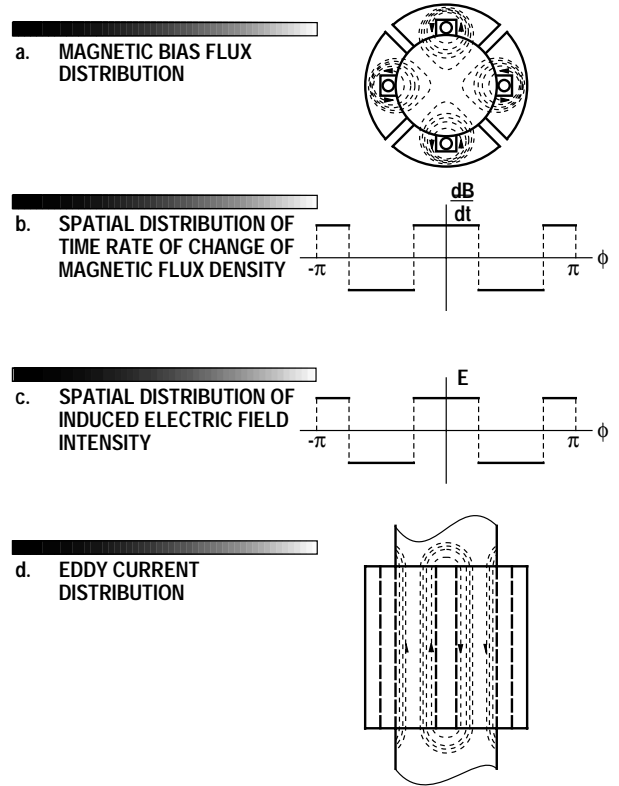


Fig. 13 Flux and eddy current distributions. (a) Magnetic bias flux distribution. (b) Spatial distribution of time rate of change of magnetic flux density. (c) Spatial distribution of induced electric field intensity. (d) Eddy current distribution

that the shorted-turn time constant of (18) represents an upper bound. The shorted-turn constant of (17) represents a lower bound for the longitudinal field case since fringing fields will lower the shorted-turn resistance for that geometry. Equations (17) and (18) imply that the shorted-turn damping constant for the transverse field device may be about 30 percent of that for the longitudinal field case. Consequently, a switching time for the transverse-field device equal to 30 percent or less of the time for an equivalent-geometry longitudinal field type should produce the same shorted-turn energy dissipation.

IV. EXPERIMENTAL VERIFICATION

To validate the theory, a phase shifter was fabricated at C-band. The basic design was that of longitudinal-field dual-mode unit using a saturation magnetization of 1200 G and a rod diameter of 0.480 in. The rod was fitted with yokes and tested as a longitudinal-field unit. The yokes were removed and new yokes designed to establish a transverse-field unit. The insertion loss envelope, as the phase shifter is switched between the various states, is shown in Fig. 14.

The measurement of switching energy was made during the set cycle. The phase shifter was saturated with a reset pulse. The drive voltage was then varied while holding the volt-time product constant, and the average current was measured. The product of average current and volt-time product yields the switching energy. The switching energy was normalized to that obtained for a switching time of 75 μ s and then plotted versus the reciprocal of the set pulse width ($1/T$). According to (16) this will yield a straight line whose slope is the shorted-turn time constant. This is shown in Fig. 15, which clearly indicates that the transverse-field device has a shorted-turn time constant that is lower by about a factor of 2.25.

V. CONCLUSIONS

A new type of dual-mode phase shifter has been described. This phase shifter uses a transverse magnetic field in the differential phase shift region. Because of the distribution of the bias field, the waveguide wall eddy currents are reduced, which results in a reduced short-turn damping time constant when compared with the conventional dual-mode unit using a longitudinal magnetic bias-field.

Analysis of the RF performance of the phase shifter was presented. This analysis indicates that the transverse-field device exhibits an optimum value of saturation magnetization which minimizes the insertion loss and that this value is considerably less than that of the longitudinal-field device. Unlike the longitudinal-field device, whose diameter is limited by the onset of higher order modes, the transverse-field device exhibits an optimum diameter which minimizes insertion loss.

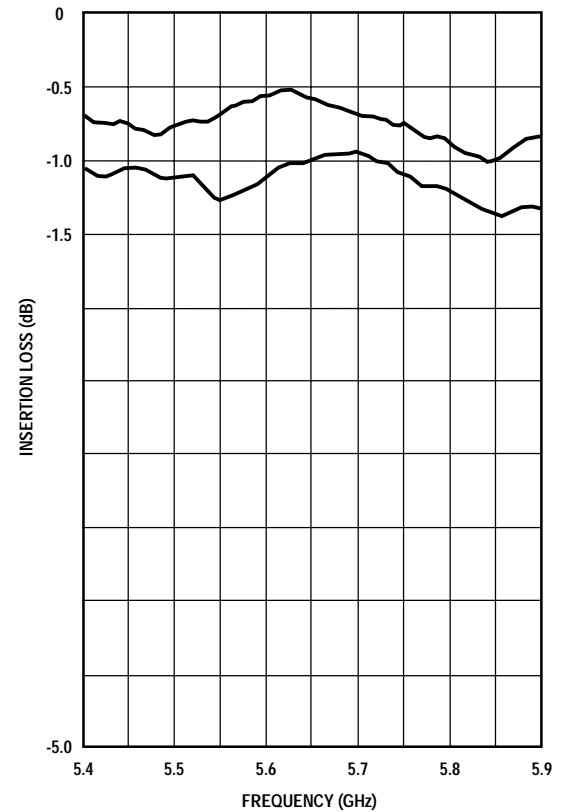


Fig. 14 Insertion loss envelope versus frequency

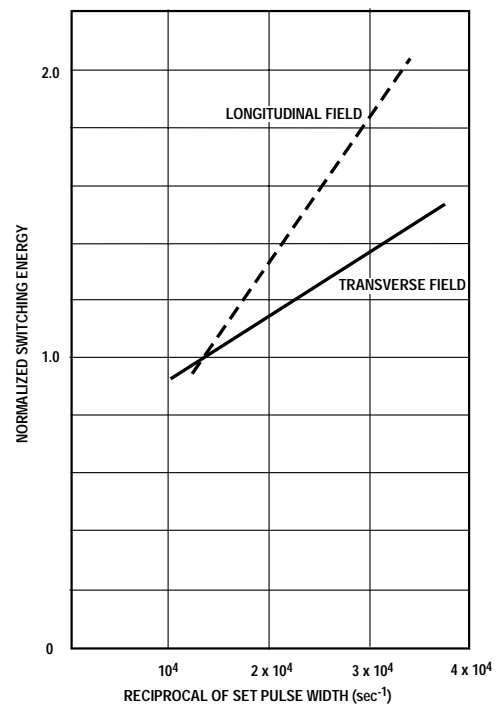


Fig. 15 Switching energy as a function of the reciprocal of switching time

V. REFERENCES

- [1] C. R. Boyd, Jr., "A Dual-Mode Latching Reciprocal Ferrite Phase Shifter", *IEEE Trans. Microwave Theory Tech.*, Vol. MTT-18, pp. 1119-1124, Dec. 1970.
- [2] R. G. Roberts, "An X-Band Reciprocal Latching Faraday Rotator Phase Shifter", in *IEEE Int. Microwave Symp. Dig.*, May 1970, pp. 341-345.
- [3] C. R. Boyd, Jr., "Design of Ferrite Differential Phase Shift Sections", in *IEEE Int. Microwave Symp. Dig.* May 1975, pp. 240-242.
- [4] C. R. Boyd, Jr., "A Transmission Line Model For The Lossless Nonreciprocal Waveguide", in *Proc. Int. Symp. Microwave Technology in Industrial Development (Brazil)*, July 1985, pp. 209-216.
- [5] J. J. Green and F. Sandy, "Microwave Properties of Partially Magnetized Ferrites", Rome Air Development Center, Rome, NY Final Report, RADC-TR-69-338, Sept. 1969.
- [6] C. R. Boyd, Jr., "Comments On The Design and Manufacture of Dual-Mode Reciprocal Latching Ferrite Phase Shifters", *IEEE Trans. Microwave Theory Tech.*, Vol. MTT-22, pp. 593-601, June 1974.